Lipus, M. P., Reinsch, T., Schmidt-Hattenberger, C., Henninges, J., Reich, M. (2018): Gravel pack monitoring with a strain sensing fiber optic cable. - *Oil Gas-European Magazine*, *44*, 4, pp. 179—185.

DOI: http://doi.org/10.19225/181202

Gravel Pack Monitoring With a Strain Sensing Fiber Optic Cable

By M. LIPUS, T. REINSCH, C. SCHMIDT-HATTENBERGER, J. HENNINGES and M. REICH*

Abstract

Achieving and maintaining borehole integrity is a challenge in the successful and sustainable utilization of hydrocarbons, geothermal energy and sites for geological storage. Information about the integrity of casing and cement is mainly available from logs which only produce data at the moment of measurement and require running in hole with logging tools. This study investigates the potential for real-time monitoring of a fiber optic distributed strain sensor, which is permanently installed behind the casing of a geothermal well. Each location of the fiber conveys information about its temperature and mechanical stress state when interacting with a laser pulse, which is sent through the fiber. This article shows field data from a gravel pack installation and compares the results to conventional borehole measurement equipment during the completion of a geothermal well. It was found that the mechanical strain acting on the fiber matches results from conventional downhole logging tools for density measurements. Both downhole cable and casing pipe experience measurable axial compression at locations where wellbore fluid is being replaced by gravel. Moreover, observation of the strain response over the initial hours post completion of the gravel packing reveals an ongoing movement of annular material (sagging and compaction of filter gravel pack).

Introduction

Geothermal energy provision might play a vital role in meeting the energy demand of modern society. One key advantage of geothermal power compared to other renewable energy resources is its high availability factor. On average, geothermal power plants are operational 75% of the time [1]. In comparison, energy from wind (21%), solar (14%), hydro (42%) and biomass (52%) are far less reliable for constant energy provision. The primary factor why geothermal energy is not permanently available is due to well intervention and maintenance of surface infrastructure (e.g. pumps and pipelines). With respect to the well, the integrity of the installed tubular casing and cement is of utmost importance during the operational lifetime of a geothermal well. In addition, subsurface stresses resulting from, e.g. reservoir compaction, can lead to severe damage to the casing pipe [2]. In sedimentary reservoirs, a gravel pack is usually installed in the open hole section between the slotted liners and the permeable reservoir horizon. It mitigates instability of the rock formation and reduces production of the sand phase [3]. Conventional borehole measurements are conducted with wireline logging tools, which require shutting in of the well and entering the borehole with sensor equipment. A possible method to optimize well interventions is by installing fiber optic cables permanently in the annulus between the casing and cement. This technology allows quasi-continuous, real-time monitoring of the subsurface infrastructure. In fiber optic sensing technology, the term distributed refers to the ability to measure anywhere along a continuous length of a sensing fiber.

Over the last two decades, much work has been published on the analysis of distributed temperature sensing (DTS) in wellbore applications to assess the thermal properties of downhole lithologies and water bearing fractures [4–6]. DTS data was further applied to perform cement job evaluations and well bore integrity analysis during and after production tests [7, 8]. Distributed strain sensing (DSS) is a collective term that comprises a range of technologies being capable of resolving mechanical strain along a fiber. The oldest and most prominent approach for quasi-distributed fiber optic strain sensing uses fiber bragg gratings (FBG). An FBG is formed by an artificial, periodic change of the refractive index n_{eff} along a defined interval of a fiber core with a grating period Λ. A narrow band of the incident optical field within the fiber is reflected by successive, coherent scattering from the index variation [9]. The strongest interaction occurs at the Bragg wavelength λ_B according to

$$\lambda_B = 2n_{eff} \Lambda \quad (1)$$

Strain sensitivity from the wavelength λ_B originates from the change in Λ due to deformation and from a change in n_{eff} due to temperature and the strain-optic effect [10]. Strictly speaking, FBG are point sensors, since the number of FBG that can be multiplexed in a single fiber is limited. The primary limiting factor for the number of gratings in a single fiber is the optical budget. Previous publications show results from a set of over 2000 gratings over a length of 190 m [11]. For true distributed strain sensors, the most prominent technology for DSS is based on Brillouin Optical Frequency Domain Analysis (BOFDA) [12]. Commercially available BOFDA systems provide a strain accuracy of 2 με at spatial resolution of 1 m up to 50 km. This technology requires access from both ends of a fiber.

The fiber optic interrogator used in this work is an optical backscatter reflectometer (Luna OBR 4400) based on the principle of Optical Frequency Domain Reflectometry (OFDR). This technique has been described in detail in previous publications [13–15]. In a nutshell, an OBR trace is a spectral fingerprint of an optical fiber at a given temperature and strain condition. Natural heterogeneity of molecules that make up the glass fiber can be interpreted as weak, randomly distributed FBG with arbitrary grating periods. Although being random, the spectral response of the backscattered light is steady and repeatable. Changing the temperature or the stress state at any interval of a fiber will lead to a linear shift in the spectral response $\Delta\nu$ of the backscattered light. The correlation between a change in temperature ΔT and the spectral response $\Delta\nu$ is caused by the thermal coefficient of the refractive index and the thermal expansion coefficient [16]. The correlation between a change in strain $\Delta\varepsilon$ and the spectral response $\Delta\nu$ is caused by length changes of the fiber. The spectral response is hence given by the following formula:

$$\Delta\nu = K_T^{-1} \cdot \Delta T + K_\varepsilon^{-1} \cdot \Delta\varepsilon \quad (2)$$

where K_T and K_ε are the temperature and strain calibration constants: K_T= 0.801°C/GHz, and K_ε=6.67 μ_ε/GHz [17]. Because of the cross sensitivity of strain and temperature, an independent temperature measurement on a separate fiber (e.g.

* Martin Lipus, Thomas Reinsch, Cornelia Schmidt-Hattenberger, Jan Henninges, GFZ German Research Centre for Geosciences, Potsdam, Germany; Matthias Reich, TU Bergakademie Freiberg, Freiberg, Germany. E-mail: mlipus@gfz-potsdam.de

0179-3187/18/IV DOI 10.19225/181202

with a DTS system or a strain free fiber) is necessary to correct for the temperature effect.

Thorough mechanical coupling of the fiber with the environment has to be given for DSS measurements, independent of which system is used for strain sensing. For example, it is not possible to quantify the behavior of a casing interval with DSS, if no bond between the two materials is given. Previous publications show that axial compression, buckling and shearing of a casing pipe can be measured when wrapping a fiber helically along the outer diameter of the pipe [11, 18]. In the published cases, fibers are either glued to the surface using epoxy resin or embedded into the material itself.

The preparation time for such an installation is high and wet connectors are used for downhole implementation to connect the prepared fiber optic installation to a fiber that connects to the read-out unit at the surface. In this study, it is shown that DSS data can be obtained from a linear fiber optic cable installation connected only to the casing by several meter spaced clamping points. The cable is a conventional downhole cable, which is not designed to pick up strain. In order to use the cable for DSS, the strain translation from the outside of a multi-layer cable to the fiber is assessed in two ways: by laboratory experiment and analytical calculation. The calibration parameters, which were determined, are later used to analyze the mechanical response of the fiber caused by gravel packing of a shallow geothermal well.

Cable Strain Calibration

A fiber optic cable for downhole application consists of rigid layers that protect the fiber from the harsh ambient conditions. These layers reduce the strain response of the fiber to external mechanical perturbations. The strain response of fiber optic cable deployed in the well in this study was accessed analytically and experimentally. A concept to estimate fiber optic coupling analytically is by calculating the mechanical stiffness of each cable component individually and adding up the values to a cable specific stiffness. Special attention is given to the viscous gel filling layer between the fiber and steel tube. Such a thixotropic fluid is used to protect the optical fibers during movement of the cable [19]. Previous studies indicate that for low shear stresses, the gel filling can be regarded as an elastic medium [20].

Typically, gels are designed to have a yield point of 35–140 Pa depending on the application [21]. Stresses below the yield strength result in elastic deformation. The stiffness k of each component is defined as the product of its cross sectional area A and its material specific Young's modulus E.

$$k = \sum_{i=1}^{n} k_i = \sum_{i=1}^{n} A_i E_i \qquad (3)$$

The Young's modulus was first introduced in Hooke's law [22] and it describes the force needed to generate a certain strain of a material:

$$\sigma = \varepsilon E \qquad (4)$$

where σ is the stress and ε the strain. With respect to the stiffness k, the stress σ is can be expressed as:

$$\sigma = \frac{F}{A} = \varepsilon \frac{k}{A} \qquad (5)$$

A sketch of the cross section of the cable used in this study is shown in the first subplot of Figure 1. The experimental approach was achieved by hanging an interval of the downhole cable vertically in a temperature stable laboratory (Fig. 1, right subplot). In order to approximate the conditions that would occur at the bottom of a shallow well with 230 m depth, a fiber optic extension of 190 m is connected in between the OBR system and the downhole cable sample, which has a length of 23 m. The cable is mechanically clamped with a vice to keep it immovable. At a distance of 1 m below the clamping point, an aluminum table is clamped to the cable. Pre-tension is applied to the cable by hanging a mass of 2 kg below the weight holder. This ensures a straightened positioning of the rigid cable to mimic the field installation. After measuring a baseline/reference trace, the weight on the aluminum table was successively increased (5 g, 10 g, 20 g, 30 g, 40 g, 60 g, 80 g, 100 g, 150 g, 200 g, 300 g). After each weight increase, one measurement was taken directly, a second measurement after 5 min and a third measurement after 10 min. The weights were subsequently removed one after another with resulting weights on the table of: 200 g, 150 g, 100 g, 40 g, 0 g.

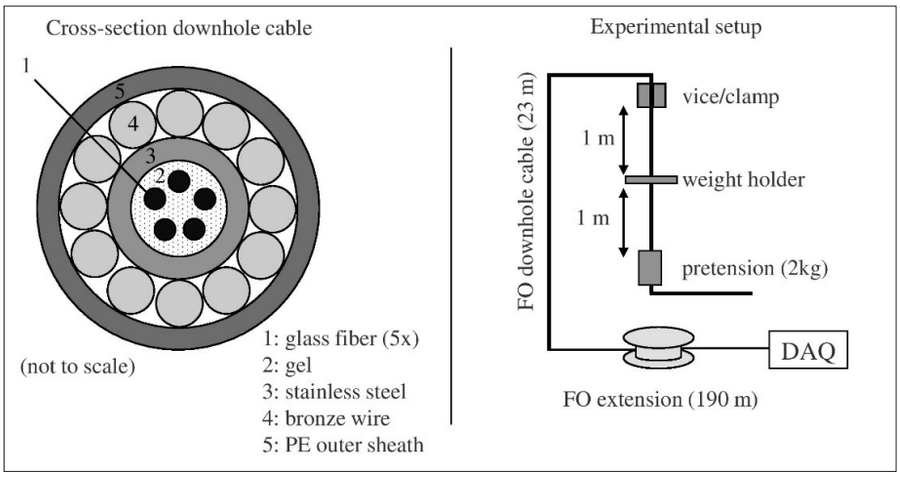

Fig. 1 Downhole cable cross section and experimental setup for strain calibration. Field cable manufactured by nkt cables GmbH

Fiber Optic Field Installation

Three fiber optic cables were installed for permanent use in a research well for aquifer thermal energy storage in Berlin (ATES Fasanenstrasse, Gt BChb 1/2015) (Fig. 2). The outermost cable was installed to a depth of 192 m and located behind a conventional 11 3/4″ steel anchor casing, which has a landing depth of 212 m. The cable was installed in a loop, so that two cable ends are accessible at the surface. During installation, the cable is fixed with a strapping machine twice per joint, one close to the coupling and one in the middle. The joints have a nominal length of ca. 11.5 m so that the cable clamping spacing is 5.75 m. Centralizers were installed at every third joint below the coupling. The anchor casing was cemented with an inner string (stinger) cementation. The cement type was class G Portland cement (CEM IIIB 32.5).

Subsequently, the well was drilled to 570 m to reach the target reservoir horizon. However, due to inadequate reservoir properties, a cement plug was pumped to develop a shallower reservoir interval from 222–227 m. The TOC of the cement plug is located at 259 m. A production casing was installed to 235 m. The production casing consists of a DN80 casing (steel grade: 1.4571, pipe thickness: 6 mm) with a 10 m wire-wrapped screen and a crossover to 6 5/8″ composite material (glass reinforced polymer). Two fiber optic cables were installed on the outside of the casing. One of the cables is installed in a loop, containing two multimode fibers and one cable single ended containing both single-mode and multimode fibers. The cables were clamped to the casing in intervals of 5 m. Additionally, two PE tubes with an OD of 4 cm

were installed, one to a depth of 211.5 m and one to 99 m. The deeper PE tube was used later for cement injection and the shallower PE tube was used to lift remaining fluids from the annulus after well completion.

A gravel pack was installed to develop the filtered interval of the well. Gravel was added into the annulus at the surface to fill the interval from the cement plug up to the transition to the anchor casing at 212 m. The required gravel volume was calculated from a caliper logging trip in the open hole section. During the gravel packing, the setting height was constantly monitored with a wireline γγ-density-log inside the production casing. Once a setting height of 213 m was reached, gravel addition and logging were stopped. A filling up to 212 m was estimated from the remaining gravel, which was still in suspension in the annulus. The subsequent cement job was scheduled for 10 hours after completing gravel packing.

Just before the start of the cementation, a quality control on the setting height of the gravel pack was performed with a γγ-density-log. The measurement revealed that the gravel head dropped by 4 m to a depth of 216 m compared to the earlier measurement. Consequently, the scheduled cementation had to be delayed by one day due to a remedial gravel packing operation. After reworking of the gravel pack, the well completion continued with cementation of the shallower interval with a TOC at 105 m through the deeper PE tube.

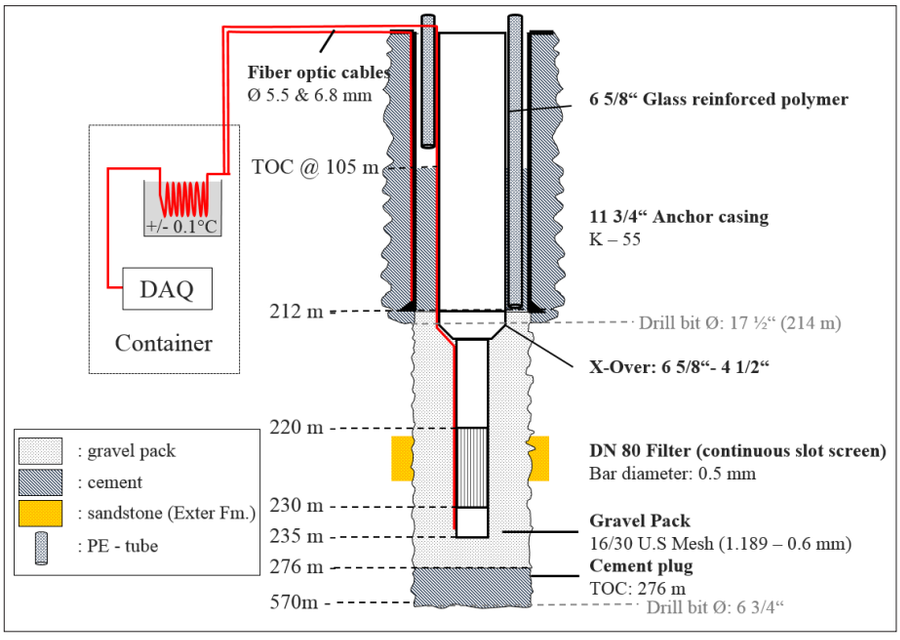

Fig. 2 Well design of the ATES Berlin (Gt BChb 1/2015) with fiber optic cable configuration after completion (not to scale)

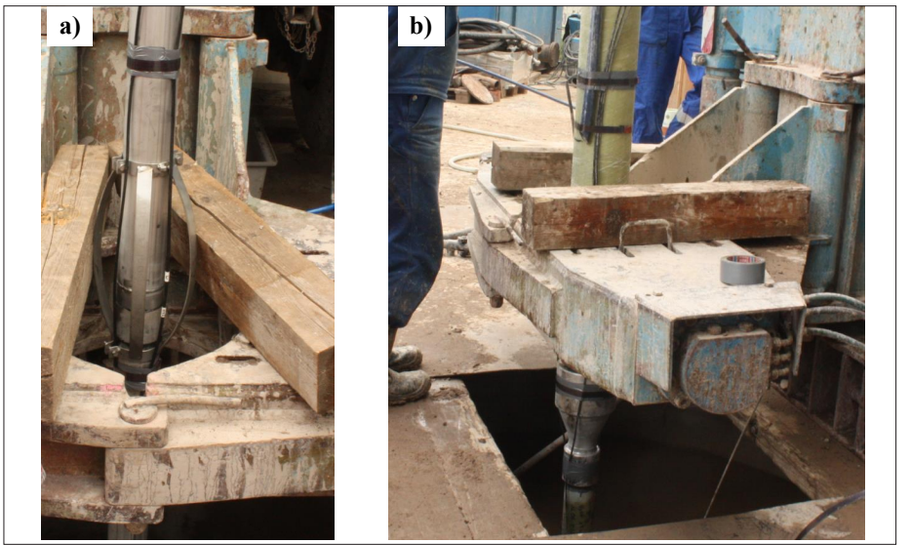

Fig. 3 a) Cable clamping configuration 2 m above shoe of production casing. Cable is secured by a centralizer (MD: 233 m). b) Cable clamping configuration at cross over from DN80 to 6 5/8”. Blue PE cement injection tube visible at the top. A centralizer above the crossover location remains hidden in this picture (MD: 211 m)

Results

First, results from the fiber optic cable calibration are shown. After that, field data from the primary gravel pack. In the third part, data after primary gravel packing and the remedial gravel packing operation are shown.

Stress transmission within a complex cable

The analytical solution for the cable cumulative stiffness k with the given cable design (Tab. 1) was calculated with Eq. 3 and 5. It resulted in a value of k = 597 ± 36 kN. For the experimental approach, the measured spectral shift Δν value was translated to strain according to Eq. 2. Figure 4 shows the correlation of the spectral response of the downhole cable to mechanical strain for the analytical and experimental approach (subplot on the right). An example of the distributed strain reading as a function of the location along the cable is shown (subplot on the left). The result indicates a good fit between the analytical calculation and experimental measurements in the investigated strain range up to 5 με (equivalent to a length change of 5 μm/m). The measured spectral shift shows a temporal variation after each weight placement. After starting with relatively high values just after weight placement, the Δν reading reduces within the next 5–10 min. It was observed, that after 10 min Δν remains constant. At low deformation of the test cable ($\varepsilon < 1 \cdot 10^{-6}$), Δν drifts strongly over time. At $\varepsilon > 1 \cdot 10^{-6}$, Δν indicates more steady and repeatable values. During weight reduction, Δν shows an even lower drift over time at each weight

Tab. 1 Design of the fiber optic cable that was installed in ATES Fasanenstrasse. Typical Young’s moduli (E) according to: [21, 23, 24]

Material	Units	ID	OD	Area A	E	k	Share
		mm	mm	mm²	kN/mm²	kN	%
glass fiber	5	–	0.13	0.06	60 [1]	18	3.1
gel	–	0.63	1.80	2.53	1e-07 [2]	3e-07	0.0
stainless steel	1	1.80	2.00	0.60	210 ± 10 [3]	125	21.0
bronze wires	12	–	0.65	3.98	110 ± 5 [3]	438	73.4
LDPE*	1	3.30	5.50	15.21	1 ± 0.84 [3]	15	2.5
*low density polyethylene						Σk = 597 ± 36	

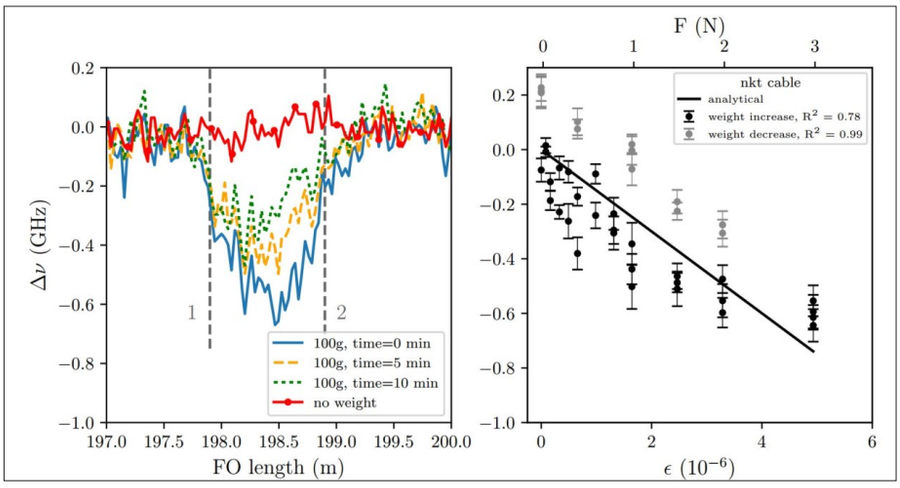

Fig. 4 Results from cable strain calibration. Left subplot: Example of a distributed strain profile during mechanical perturbation over an interval of 1 m with a mass piece of 100 g for different times after weight placement (1 – top clamping location, 2 – weight holder). Right subplot: analytical and experimental result of the correlation of strain over spectral shift for the available down-hole cable

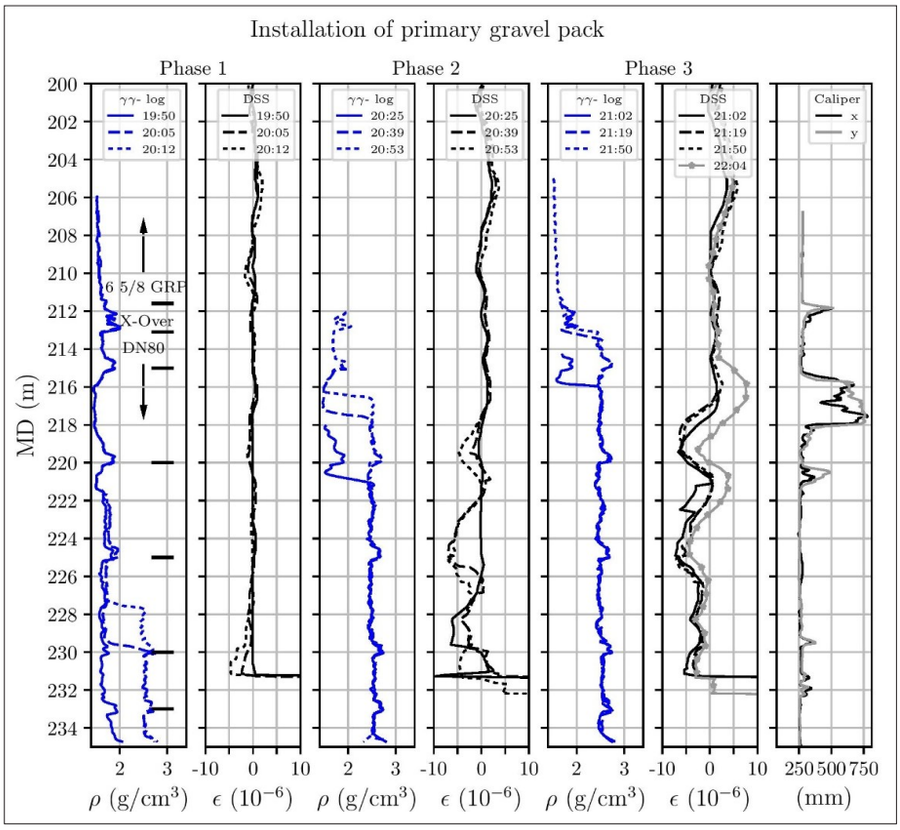

Fig. 5 Comparison of γγ-logging and DSS downhole monitoring data during gravel packing. DSS profiles are calculated relative to the mechanical state of a DSS reference trace measured at 19:40. Black horizontal lines in first subplot mark locations of joints and cable clamping location. These locations mark the points where strain signals on the cable are mechanically isolated from each other. The last subplot depicts the borehole geometry

step. There is also a better linear regression between Δν and ε during weight reduction, indicated by the R2 values. The experiment shows that a withdrawal of a mechanical load to initial conditions results in an offset. An apparent fiber elongation of 1.5 με was observed on returning back to 0 g for the measurement after 10 min. The linear regression with an error defined by the standard deviation for the increasing weights is –0.086 ± 0.009 GHz/με including all values at 0,5 and 10 min. During weight reduction this value is –0.129 ± 0.004 GHz/με. It was also observed, that the strain signal is not only confined to the stretched interval, but also enters regions beyond the clamping location by up to 20 cm. In these locations, no hysteresis was observed and the strain readings returned to the initial state.

Strain response during primary gravel packing

Figure 5 shows the downhole data that was gathered during the gravel packing of Gt BChb 1/2015. The subplots show pairs of γγ-profiles and DSS measurements that were gathered contemporaneously. The γγ-profile at the start (19:50) shows a low density below 2 g/cm³ over the interval of 206 m to 235 m. Local density spikes display the connectors of the casing joints where the fiber optic cable is clamped to the casing. Over time, the gravel head shows by the γγ-data an increase in density to 2.5 g/cm³. The last profile (21:50) shows that the setting height of the gravel pack lies at 213 m. The DSS profiles show that the gravel pack generates a negative strain signal on the cable (cable relaxation/compression). The location of the strain signal correlates to the setting height of the gravel pack. The strain profiles are segmented into intervals, which match the clamping points of the cable to the casing. A strain response has a local maximum in between two casing clamps. The cable relaxation from gravel lies between 4–8 με. The final setting height of the gravel lies in between two cable-clamping points with a narrower spacing (213 and 215 m). The maximum stretching in this interval is 2 με.

15 minutes after completing the γγ-logging, an abrupt change in the stress state of the downhole cable is observed at the depth interval 215–228 m (grey profile with marker in 6th subplot). From the clamping point at 215 m going downwards, the cable enters a tensional regime. Temperature that were measured with DTS (Fig. 7) show no response to the gravel packing and overall temperature variations do not exceed 0.2 °C (equivalent to a strain value of 1 με). Consequently, the spectral response of the DSS data is dominated by mechanical nature.

The caliper reading shows the borehole geometry in the open hole section prior to the gravel packing (far right on Fig. 5). In the interval 215–218 m, a washout exists, where the borehole diameter locally enlarges by a factor 3.

Strain response after primary gravel pack

Figure 6 shows the data that was gathered after the primary gravel packing and γγ-logging stopped. During this time no work was carried out on the well site and the borehole was shut-in. Simultaneously the well temperature increased by 1°C (equivalent to a strain value of 5.5 με) in the interval 222–228 m. The DSS signal

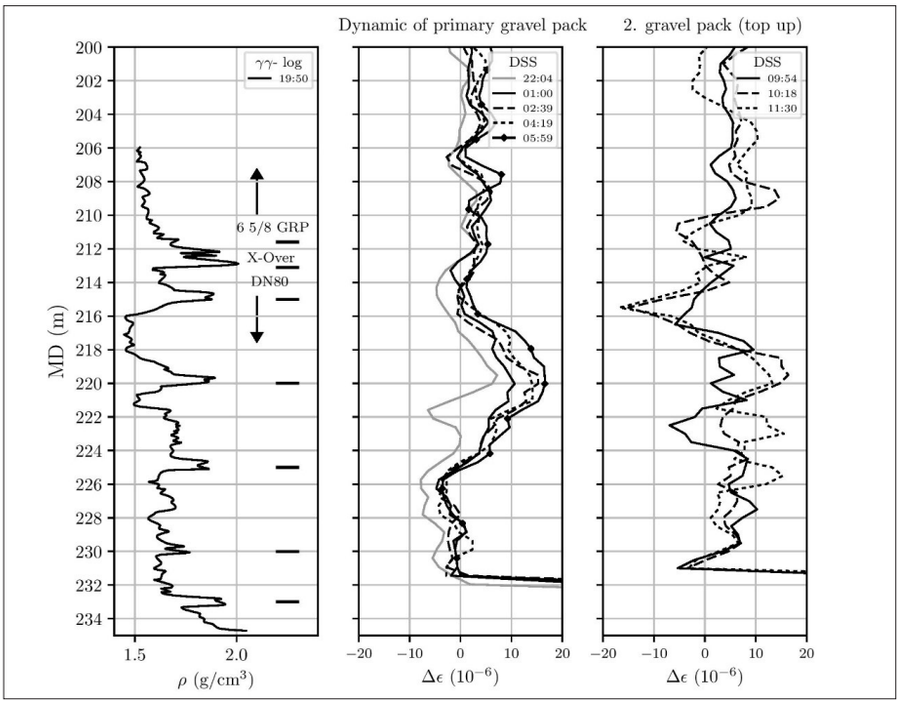

Fig. 6 Fiber optic response hours after the primary gravel packing and during the adjustment of the gravel head on the subsequent day. DSS is corrected with DTS data to infer the pure mechanical component of the measurement. For comparison, the last DSS trace from Figure 5 (22:04) is depicted in grey. The reference trace for all traces depicted here is the same as during the primary gravel packing

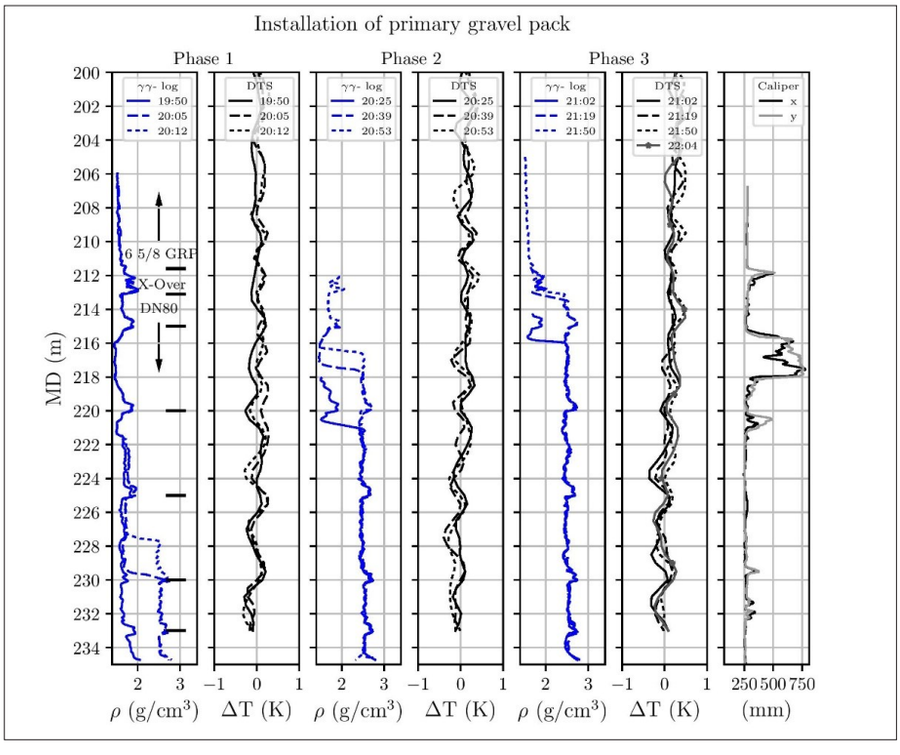

Fig. 7 Comparison of γγ-logging and relative DTS downhole monitoring data during gravel packing. Just as in the DSS plot of the gravel packing (Fig. 5), temperatures are calculated relative to the DTS trace measured at 19:40. Black horizontal lines in first subplot mark locations of joints and cable clamping locations. Temperature variation does not exceed 0.2 °C. The last subplot depicts the borehole geometry

shows a continuous increase in strain over time in the interval 216–225 m up to 18 με. Areas above and below that show no change in the stress state of the fiber optic cable.

During adjustment of the gravel pack the following morning, the DSS shows a relaxation/compression at the location where the gravel is present up to a depth of 211 m.

Discussion

Cable performance

The fiber optic cable, which was tested and deployed in the field was not initially designed to measure strain. The gel filling between the fibers and the steel tube and various different surrounding materials result in a complex mechanical interaction across the cable layers. The laboratory experiment shows hysteresis when removing a mechanical load on the cable. The likely reason for that is that the gel filling deformed plastically during elongation. During relaxation of the cable, the gel movement is probably the driving factor that created an apparent compression of the cable. The cable shows a better performance during weight reduction than during an increase in load, as depicted by the R^2 value.

The stiffness values k_i for each cable layer from Table 1 are used to calculate the force at the surface of the optical fiber, i.e. the interface to the gel filling, and the interface of the gel filling with the surrounding steel tube. At an elongation of the cable by 6 με, the shear stresses are calculated to be 11 Pa and 4 Pa, respectively. These values are a factor 3 lower that the lowermost reported yield strength for gels. Nevertheless, the mechanical deformation of the cable is measured over several minutes to hours. Over these timescales, a plastic deformation is likely to occur, as observed during mechanical load change in the field experiment (Fig. 4). These are strong indications for a differential movement between the fiber and surrounding rigid layers due to plastic gel flow. Exemplary, the DSS trace also shows that the fiber strain response goes beyond the clamping location of the vice and weight holder during load changes. Although these areas are mechanically isolated from the strained interval, the fiber experiences a tensional force. This is an important feature with respect to the analysis of the field data, where clamping locations are regarded as a mechanical isolation.

Cable buoyancy change during gravel packing

Results from the primary gravel packing show a match between the wire-line γγ-density-log and fiber optic DSS data. At the location where gravel has settled down, a relaxation of the fiber optic cable is observed. At locations where the cable is clamped to the casing, the DSS strain response tends to remain unchanged and unaffected by the gravel. In the crossover location from DN 80 production casing to 6 5/8″ composite material, the cable was clamped to the casing in very short intervals (211–215 m) to prevent damage during installation (Fig. 3). Because of that, the fiber is much more mechanically isolated than in adjacent locations.

However, as shown by the laboratory analysis, clamping locations do not isolate a mechanical signal completely due to plastic gel movement in the cable. The clamping locations at 220 m and at 225 m show a peak strain relaxation right at the clamping location, which is only possible with a strain translation beyond the clamping point. In the following, an explanation for the fiber optic relaxation is given by calculating the reduction of gravitational forces on the cable due to the gravel pack. The fiber optic cable has a weight of 63 kg/km and a diameter of 0.55 cm. Hence its density is 2.65 g/cm³. The well bore fluid prior to the gravel packing has a density of 1 g/cm³ and the average clamping point distance of the cable to the casing is 5 m. With the given parameter, the maximum apparent weight can be calculated. While being submerged in fresh water, a maximal static gravitational force of 2 N acts on the cable at the top clamping location. This additional force acts on the fiber when the reference baseline measurement is taken. A subsequent removal of that gravitational force would lead to a relaxation/apparent compression of the cable leading to a $\Delta\nu$ of 0.5 GHz and a strain (relaxation) of 4 με. These values match the measured DSS readings during gravel packing, which are in the range of 4–7 με. Instead of hanging freely in the liquid column, the cable is embedded in gravel, which compensates the gravitational pull.

At the same time the well tubular material experiences axial loading due to the pull force of the casing. The casing shoe of the production casing (235–230 m) induces a mechanical stress of 340 kPa on the wire-wrapped screen (230–220 m) while being submerged in well bore fluid with a density of 1 g/cm³ (Eq. 5). Like the downhole cable, the casing pipe will experience axial compression due to the replacement of fluid by gravel. Assuming the force to be evenly distributed over the cross sectional area of the wire-wrapped screen and using a Young's modulus for steel of 200 GPa, the strain results in 2 με (Eq. 5). The assumptions used for this calculation underestimate the actual strain, since the mechanical stress will focus on a smaller cross sectional area due to the helical geometry of steel within the wire-wrapped screen. The increase in mechanical stress will hence increase deformation of the pipe.

Cable tension due to gravel sagging and compaction

The well completion schedule was delayed by one day due to installation of a remedial gravel pack. Subsequent consolidation of the gravel head after the primary gravel pack was detected by the DSS data. DSS data, which was gathered continuously, shows an abrupt stress state change of the fiber optic cable shortly after termination of the γγ-density-log (see trace 22:04 in Fig. 5). The cable experiences extension in the interval between 215–223 m. This could be explained by a sudden consolidation of the gravel. The caliper reading shows a severe wash-out between 215–218 m. It is probable that gravel kept consolidating and additionally filled empty voids which were not filled with the primary gravel pack. Next to that, the tension on the cable increases over night, indicating steady and continuous compaction of the gravel inside the annulus in the interval from 216–225 m. DSS measurements during the secondary remedial gravel pack show a similar cable relaxation from 210–216 m as observed during primary gravel packing.

Conclusions and Outlook

This study shows a match of DSS data and conventional wireline γγ-density-logging data. That is because the cable and the casing pipe experience axial compression when the surrounding liquid is being replaced by gravel. Even though the cable relaxation is as small as 6 μm/m, it is readily detectable with the fiber optic interrogator. In addition, the continuous DSS logging reveals subsequent sagging and compaction of the annular material in real-time after the wireline logging terminated. This study also shows that DSS data can be acquired and analyzed quantitatively, even for a cable of non-optimized design. However, for future installations it is recommended to utilize a cable designed for strain sensing in order to mitigate the hysteresis during load changes and to further improve the spatial and strain resolution. Strain monitoring of the gravel packing is just the very first operation measured with the fiber optic cable installation. The next step will be to analyse the strain data measured during the subsequent cementation of the production casing. Over the lifetime of this well, DSS monitoring can be applied whenever required.

Acknowledgements

This study has received funding from the European Union's Horizon 2020 research and innovation program under grant agreement No 654497 (GeoWell project) and the German Federal Ministry for Economic Affairs and Energy (BMWi) under funding code 03ESP409A.

References

[1] L. Rybach: Status, development and prospects of geothermal energy, President, International Geothermal Association (IGA) (2008).

[2] K. Furui, G. Fuh, N. Morita: Casing- and screen-failure analysis in highly compacting sandstone fields, SPE Drilling and Completion, Volume 27, Issue 02 (2012).

[3] R. Saucier: Considerations in gravel pack design, SPE Journal of Petroleum Technology, Volume 26, Issue 2 (1974).

[4] E. Hurtig: Fibre-optic temperature measurements in shallow boreholes: Experimental application for fluid logging, Geothermics, Volume 23, Issue 4 (1994).

[5] A. Foerster, J. Schroetter, J. Merriam: Application of optical fiber temperature logging - an example in a sedimentary environment, Geophysics, Volume 62, Issue 4 (1997).

[6] J. Henninges, E. Huenges, H. Burkhardt: In situ thermal conductivity of gas-hydrate-bearing sediments of the mallik 5l-38 well, Journal of Geophysical Research (Solid Earth), Volume 110, Issue B11 (2005).

[7] T. Reinsch: Thermal, mechanical and chemical influences on the performance of optical fibres for distributed temperature sensing in a hot geothermal well, Environmental Earth Sciences, Volume 70, Issue 8 (2013).

[8] C. Buecker, S. Grosswig: Distributed temperature sensing in the oil and gas industry - insights and perspectives, Oil Gas European Magazine, Volume 43, Issue 4 (2017).

[9] K. Hill, G. Meltz: Fiber bragg grating technology fundamentals and overview. Journal of Lightwave Technology, Volume 15, Issue 8 (1997).

[10] A. Bertholds, R. Dandliker: Determination of the individual strain-optic coefficients in single-mode optical fibres, Journal of Lightwave Technology, Volume: 6 Issue: 1 (1988).

[11] F. Rambow, D. Dria, B. Childers, M. Appel, J. Freeman, M. Shuck, S. Poland: Real-time fiber-optic casing imager. SPE Journal, Volume 15, Issue 4 (2010).

[12] D. Garcus, T. Gogolla, K. Krebber, F. Schliep: Brillouin optical-fiber frequency-domain analysis for distributed temperature and strain measurements, Journal of Lightwave Technology, Volume 15, Issue 4 (1997).

[13] B. Soller, D. Gifford, M. Wolfe, and M. Froggatt: High resolution optical frequency domain reflectometry for characterization of components and assemblies, OPTICS EXPRESS, Volume 13, Issue 2 (2005).

[14] E. Moore: Advances in Swept-Wavelength Interferometry for Precision Measurements, Ph. D. thesis, Department of Electrical, Computer, and Energy Engineering, University of Colorado (2001).

[15] S. Liehr, K. Krebber, Application of Quasi-Distributed and Dynamic Length and Power Change Measurement Using Optical Frequency Domain Reflectometry, IEEE Sensors Journal, Volume 12, Issue 1 (2012).

[16] T. Priest, K. Jones, G. Scelsi, G. Woolsey: Thermal coefficients of refractive index and expansion in optical fibre sensing, 12th International Conference on Optical Fiber Sensors, paper OWC41. Optical Society of America (1997).

[17] M. Froggatt, J. Moore: High-spatial-resolution distributed strain measurement in optical fiber with Rayleigh scatter. Applied Optics, Volume 37, Issue 10 (1998).

[18] D. Earles, C. W. Stoesz, N. Surveyor, J. G. Pearce, H. A. DeJongh: Fiber optic strain sensing at the sand face enables real-time flow monitoring and compaction mitigation in openhole applications. SPE Annual Technical Conference and Exhibition, 30 October-2 November, Denver, Colorado, USA (2011).

[19] S. Khan, S., M. Maruca, I. Plitz: Rheology of fumed silica dispersions for fiber-optic cables. Polymer En-

gineering & Science, Volume 31, Issue 24 (1991).
[20] T. Reinsch, T. Thurley, P Jousset: On the coupling of a fiber optic cable used for distributed acoustic/vibration sensing applications - a theoretical consideration. Measurement Science Technology, Volume 28, Issue 12 (2017).
[21] Evonik Industries: Aerosil fumed silica for cable gels, technical information 1163, technical report, Evonik Industries (2015).
[22] R. Hooke: Lectures de Potentia Restitutiva, Or of Spring Explaining the Power of Springing Bodies. John Martyn (1678).
[23] H. Kuchling Taschenbuch der Physik. Carl Hanser Verlag GmbH & Co. KG (2011).
[24] F. Cardarelli: Materials Handbook, A Concise Desktop Reference, 2nd Edition. Springer (2008).

M.Sc. Martin Lipus studied Petroleum Engineering at the TU Delft (NL). Since 2016 he has been working as a PhD student at the GFZ Potsdam with a focus on distributed strain sensing for wellbore integrity monitoring.

Dr.-Ing. Thomas Reinsch is a research scientist at GFZ working on fiber optic sensing technologies for wellbore applications. He studied physics and geology at University of Cologne and has PhD degree in petroleum engineering from Clausthal University of Technology.

Dr. Cornelia Schmidt-Hattenberger holds a doctoral degree in Physics from Friedrich-Schiller-University Jena. She has over 20 yrs. experience in development and application of sensors for geotechnical projects. She joined the GFZ Potsdam in 1993 and worked in the fields of scientific instrumentation, rock mechanics and environmental geotechnics.

Dr. Jan Henninges holds a doctroral degree in the field of Applied Geophysics from TU Berlin. Since 2001 he is research scientist at GFZ. His research is focused on monitoring of dynamic subsurface processes, particularly applying fiber-optic sensing techniques in boreholes.

Prof. Dr.-Ing. Matthias Reich studied process engineering at the TU Clausthal. He worked as a development and product engineer for Baker Hughes from 1986 till 2006. Since 2006 he holds the chair for Drilling Engineering and Mining Machinery at the TU Bergakademie Freiberg.